

Supporting Information

**Efficient n-type dopants with extremely low doping ratios for high performance inverted perovskite solar cells**

Zhengyang Bin,<sup>†</sup> Jiangwei Li,<sup>†</sup> Lian Duan,\* Liduo Wang\*

<sup>†</sup> These authors contribute equally to the work.

Key Lab of Organic Optoelectronics & Molecular Engineering,

Department of Chemistry, Tsinghua University, Beijing, 100084, P. R. China

E-mail address: [duanl@mail.tsinghua.edu.cn](mailto:duanl@mail.tsinghua.edu.cn), [chldwang@mail.tsinghua.edu.cn](mailto:chldwang@mail.tsinghua.edu.cn)

## 1. Experimental methods

**Theoretical Calculations:** The geometrical and electronic properties of formed organic radicals were performed with the Gaussian 03 program package. The calculations were optimized by means of B3LYP (Becke three parameters hybrid functional with Lee–Yang–Perdew correlation functionals) with the 6-31G(d) atomic basis set. The molecular orbitals were visualized using Gaussview.

**Device Fabrication:** All the chemicals were used as received, including PbI<sub>2</sub> (99.9985%, Alfa Aesar), CH<sub>3</sub>NH<sub>3</sub>I (Dysol), nickel acetylacetonate (96%, J&K), Magnesium acetatetetrahydrate (99%, Sigma Aldrich), lithium acetate (99%, Sigma Aldrich), PC<sub>61</sub>BM (99.5%, Lumtec Co., Taiwan). Solvents of acetonitrile, ethanol, dimethylsulfoxide, chlorobenzene,  $\gamma$ -butyrolactone and isopropanol were all purchased from Sigma Aldrich. FTO glasses (YINGKOU OPV TCH NEW ENERGY CO., LTD, OPVFTO22-7) were etched with zinc powder and 1 M HCl to obtain the electrode pattern, and then washed with cleaning fluid, deionized water, ethanol, acetone and isopropanol sequentially. The NiMgLiO layer was obtained with a ~20nm thickness by spray pyrolysis as reported. Then the substrates were transferred to the glove box (H<sub>2</sub>O content lower than 0.01 ppm) for perovskite deposition. The perovskite solution was prepared with 1 M PbI<sub>2</sub> and CH<sub>3</sub>NH<sub>3</sub>I in GBL/DMSO (7:3) mixed solvent and stirred at 70 °C overnight. 80  $\mu$ L solution was spread on the FTO/NiMgLiO substrate followed by a two-stage spin-coating process (1000 rpm for 10 s and 4000 rpm for 30 s). 500  $\mu$ L chlorobenzene was dripped as anti-solvent 15 s after the second stage to obtain a light-brown smooth perovskite thin film. Then the substrates were annealed at 70 °C for 30 min to convert to a dark-brown film. 15 mg/ml chlorobenzene solution of PCBM was spin-coated on the cooled substrates at 1500 rpm for 30 s, followed by the spin coating of BCP saturated solution in isopropanol. Finally, a 120 nm Ag electrode was thermally evaporated on top of the device under high vacuum ( $<10^{-4}$  Pa). For the n-doped PCBM, stock solutions of H1, H2 and H3 were prepared with a 5 mg/ml concentration and a corresponding volume of stock solution was added to obtain an n-doped ETM solution. The active area of the device was 0.09 cm<sup>2</sup>, defined by the aperture area of the mask.

**Measurements:** <sup>1</sup>H NMR spectra were measured on a JEOLAL-600 MHz spectrometer at ambient temperature with tetramethylsilane as the internal standard. Mass spectra were recorded on a Bruker Esquire iontrap mass spectrometer. ESR spectra are measured at the ambient temperature on the JES-FA200 ESR Spectrometer. Measurement conditions: (1) magnet field: sweep time is 1.0 min, center

field is 324.3 mT, and sweep width is 5\*1 mT. (2) microwave: frequency is 9058.8 MHz, power is 0.998 mW, phase is 340, and coupling is 599. The PCBM and n-type doped PCBM samples are dissolved in deoxygenated toluene solution of 10 mg/mL with the same doping ratio of 5%. To compare the spin concentration of PCBM samples with different n-type dopants, all the other conditions are kept the same, including doping concentration, solution volume, the height of the sample tube, and also the same measurement conditions. Absorption spectra were recorded with an UV-vis spectrophotometer (Jobin Yvon, FluoroMax-3). The time-resolved PL spectra were measured using an Edinburgh Instruments FLS920 spectrometer by the time correlated single photon counting (TCSPC) technique. An EPL 515 nm pulsed diode laser was used for excitation with repetition rates at 10MHz. The maximum average power was 5 mW and all samples were measured at the same intensity with an instrument response function (IRF). The emission wavelength was set at 765 nm. The ultraviolet photoelectron spectroscopy (UPS) characterizations were carried out with monohromatized HeI radiation at 21.2 eV. The work function of samples were determined according to  $WF = h\nu - Be_{SEE}$ , where  $Be_{SEE}$  is the binding energy relative to the Fermi level of the calibrated spectrometer that corresponds to the secondary electron cutoff, and  $h\nu$  is the HeI photon energy. SEM images were acquired with a field-emission scanning electron microscope (FE-SEM, JEOL JSM-7401F). The photocurrent-voltage (J-V) characteristics of the devices were measured with a Keithley 2400 digital source meter at the scan speed of 100 mV/s. The simulated AM 1.5 sunlight with an irradiance equivalent to 100 mW/cm<sup>2</sup> was generated by an thermo oriel 91192-1000 simulator and the intensity was calibrated with an VLSI standards incorporated PN 91150V Si reference cell.

## 2. Molecular design

Introducing donating group of -MeO at the benzene ring can increase the electron density around benzene ring, leading to a higher SOMO energy level of DMBI radicals. Therefore, molecules based on DMBI structure are designed according to the position and numbers of -MeO group. The SOMO energies are summarized in **Table S1** and the molecular structures are listed in **Figure S1 (a)**.

**Table S1.** SOMO energy of DMBI molecules.

Molecular design	Molecular structure	Energy level of SOMO / eV
Position of MeO	<i>o</i> -MeO	-2.53
	<i>m</i> -MeO	-2.69
	<i>p</i> -MeO	-2.54
SOMO Energy: $o \approx p > m$		
Numbers of MeO	2,6-Di-MeO	-2.29
	2,4-Di-MeO	-2.36
	2,4,6-Tri-MeO	-2.10
SOMO Energy: $Tri\text{-MeO} > Di\text{-MeO} > MeO$		

Firstly, the SOMO energy is changed as the position of -MeO group at benzene ring moves. As we can see from **Figure S1 (b)**, the SOMO of DMBI is mainly located at the *o*- and *p*- position of right benzene ring compared with its *m*- position. Thus introducing an electron-donating group of -MeO in the *o*- and *p*- position could largely increase its SOMO energy, as shown in **Table S1**. Secondly, with the number of -MeO group increases in the *o*- and *p*- position of benzene ring, the SOMO energy could be further improved, giving a more prospective capacity to donate electrons.

**Figure S1.** (a) Designed DMBI molecules. (b) Electron density plots of SOMO energy.

### 3. Synthesis and characterization of designed molecules

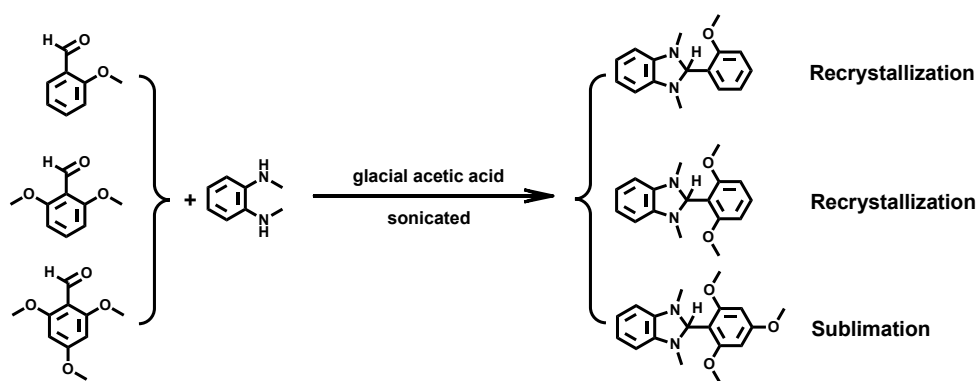


**Figure S2.** Synthetic routes for H1, H2 and H3

### Synthesis and characterization of H1 and H2

Following a literature procedure, to a mixture of *N,N'*-dimethyl-*o*-phenylenediamine (1g, 7.34 mmol), aromatic aldehyde (7.34 mmol), one drop of glacial acetic acid was then added. The reaction mixture was sonicated at room temperature until precipitation was observed. The resulting precipitate was filtered and then washed with ethyl alcohol. The pure product of H1 and H2 was received from recrystallization with ethyl alcohol.

### Synthesis and characterization of H3

Different from H1 and H2, H3 is more reactive in solution and easily be oxidized, thus could not given by recrystallizing at a relatively high temperature. Similar as the literature procedure, to a mixture of *N,N'*-dimethyl-*o*-phenylenediamine (1g, 7.34 mmol), aromatic aldehyde (7.34 mmol), one drop of glacial acetic acid was then added. The reaction mixture was sonicated at room temperature until precipitation was observed. The resulting precipitate was filtered and then washed with ethyl alcohol. The crude product was purified directly by sublimation in vacuum.

**H1:**  $^1\text{H}$  NMR (600 MHz,  $\text{CDCl}_3$ )  $\delta$ /ppm: 7.82 (d, 1H), 7.34 (dd, 1H), 7.04 (dd, 1H), 6.94 (d, 1H), 6.69 (m, 2H), 640. (m, 2H), 5.62 (s, 1H), 3.84 (s, 3H), 2.58 (s, 6H).  $^{13}\text{C}$  NMR (151 MHz,  $\text{CDCl}_3$ )  $\delta$ /ppm: 158.89, 142.47, 129.79, 129.49, 127.17, 121.20, 119.01, 110.50, 105.48, 85.02, 55.50, 33.30. MS (ESI) [ $m/z$ ] 253.14 (M-[R1]) $^+$ .

**H2:**  $^1\text{H}$  NMR (600 MHz,  $\text{DMSO-d}_6$ )  $\delta$ /ppm: 7.29 (dd, 1H), 6.68 (d, 2H), 6.43 (m, 2H), 6.18 (m, 2H), 6.16 (s, 1H), 3.62 (s, H), 2.42 (s, 6H).  $^{13}\text{C}$  NMR (151 MHz,  $\text{DMSO-d}_6$ )  $\delta$ /ppm: 160.8, 143.51, 130.86, 117.78, 112.27, 105.21, 103.72, 81.89, 56.50, 32.68. MS (ESI) [ $m/z$ ] 283.14 (M-[R1]) $^+$ .

**H3:**  $^1\text{H}$  NMR (600 MHz,  $\text{CDCl}_3$ )  $\delta$ /ppm: 6.56 (m, 2H), 6.23 (m, 2H), 6.14 (s, 2H), 6.12 (s, 1H), 3.82 (s, 3H), 3.68 (s, 6H), 2.54 (s, 6H).  $^{13}\text{C}$  NMR (151 MHz,  $\text{CDCl}_3$ )  $\delta$ /ppm: 161.49, 143.40, 117.58,

106.11, 103.55, 82.16, 56.21, 55.33, 32.70. MS (ESI) [ $m/z$ ] 313.15 (M-[R1])<sup>+</sup>.

#### 4. Conductive AFM measurement

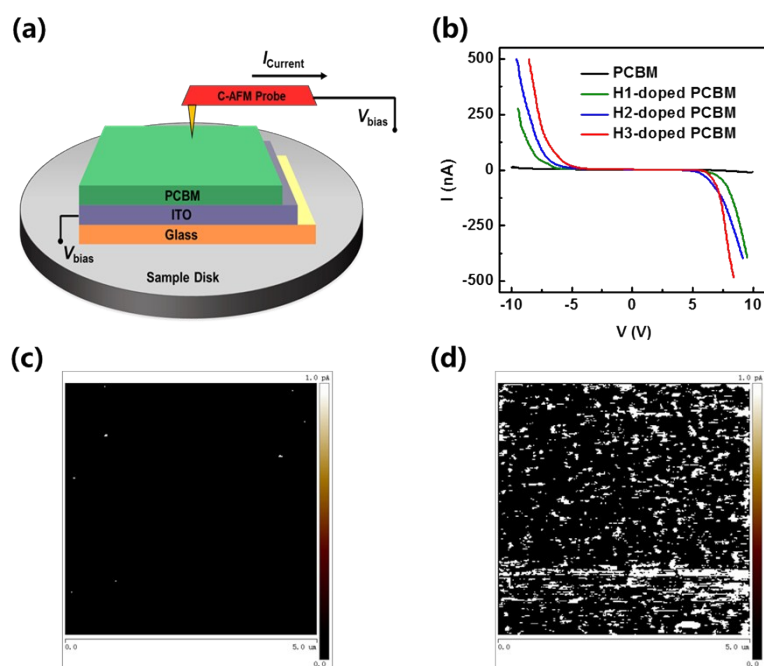


**Figure S3.** Schematic diagram of c-AFM measurements. (b) I-V curves of PCBM and n-doped PCBM measured by c-AFM. c-AFM images of (c) PCBM and (d) H3-doped PCBM films at  $V_{\text{bias}} = -5.0$  eV.

#### 5. SCLC mobility measurement

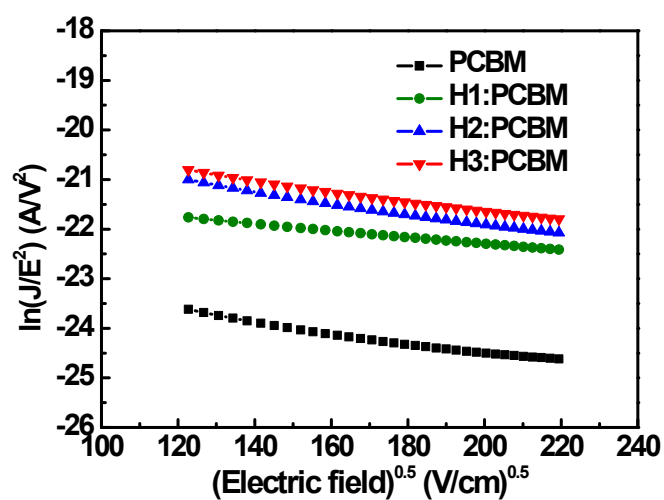


**Figure S4.** Current density-voltage data of electron-only devices

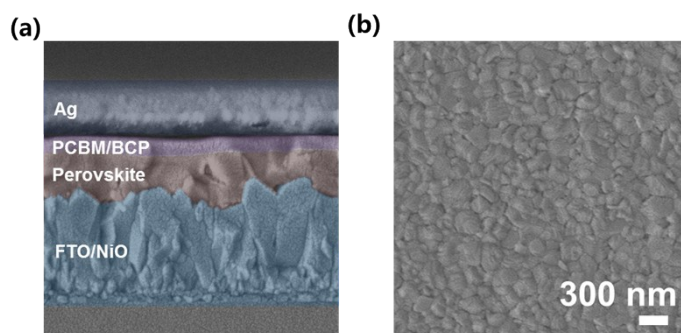
The electron mobility was approximated using space charge limited current (SCLC) measurement in which device structures were ITO/TiO<sub>2</sub>/PCBM or n-typed doped PCBM/Cs/Al. Then J-V characteristics of electron-only devices were measured from SCLC equation and Poole-Frenkel equation

$$J = \frac{9}{8} \varepsilon \varepsilon_0 \frac{E^2}{L} \mu_0 \exp(\beta \sqrt{E}),$$

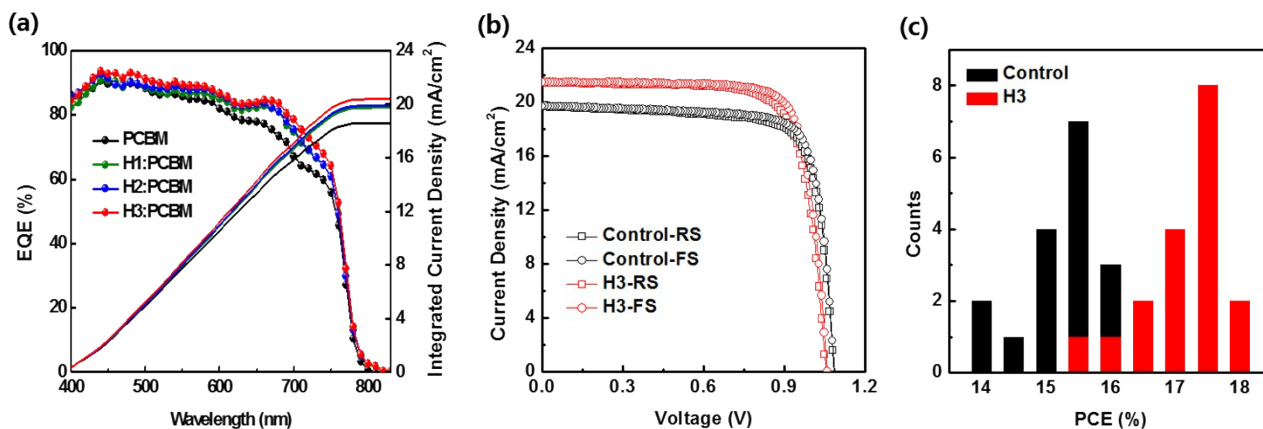
Where E is the electric field,  $\varepsilon$  and  $\varepsilon_0$  are the relative dielectric constant and the permittivity of the free space, respectively, and L is the thickness of the organic layer, and  $\beta$  is Poole-Frenkel factor, and  $\mu_0$  is the zero-field mobility.

Figure S3 shows the logarithm of  $J/E^2$  versus the square root of the mean electric field. Thus it is easy to obtain that the mobility of pure PCBM film was 0.012 cm<sup>2</sup>/Vs. Doped with n-type dopant, the mobility of PCBM films was increased to 0.068, 0.21, and 0.24, with H1, H2 and H3 respectively. The result exhibited that the charge transport in PCBM film was largely enhanced with n-typed dopants.

## 6. Supplementary evidences for the precursor solution and n-doped devices



**Figure S5.** (a) Cross-sectional SEM image of the inverted PSC. (b) Top-view SEM image of the CH<sub>3</sub>NH<sub>3</sub>PbI<sub>3</sub> thin film.



**Figure S6.** (a) EQE and integrated current densities of undoped and 0.05 w% n-doped PSCs (corresponding to the devices in Figure 3c). (b) Hysteresis characteristics (RS: reverse scan from  $V_{OC}$  to  $J_{SC}$ , FS: forward scan from  $J_{SC}$  to  $V_{OC}$ ) and (c) Histograms of PCE measured for 36 devices based on PCBM and 0.05 wt% H3-doped PCBM.

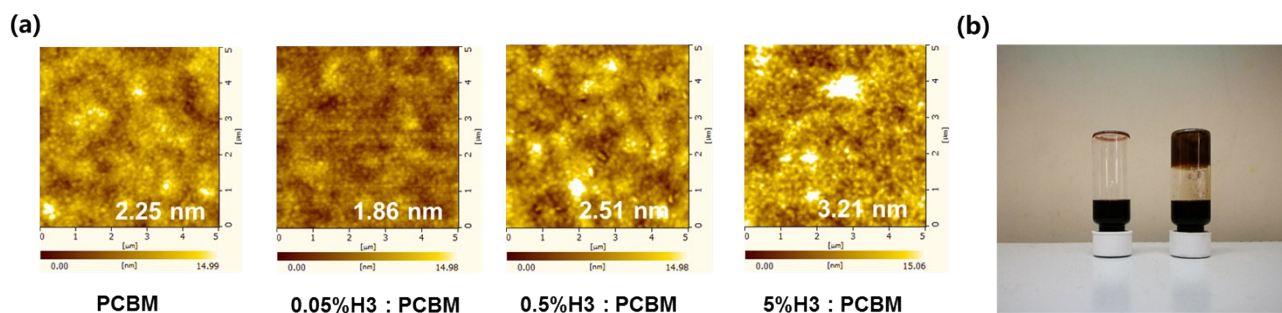


**Figure S7.** (a) AFM images of perovskite, PCBM on perovskite, and H3-doped PCBM on perovskite with varied dopant concentrations. (b) Photographs of PCBM (left) and 10 w% H3-doped PCBM solution (right). The electron transfer product of H3:PCBM is less soluble in the chlorobenzene solution, leading to rough surface morphology of the thin films and bad interfacial contact, thus causing a lowered FF of device with a large amount of n-dopant.

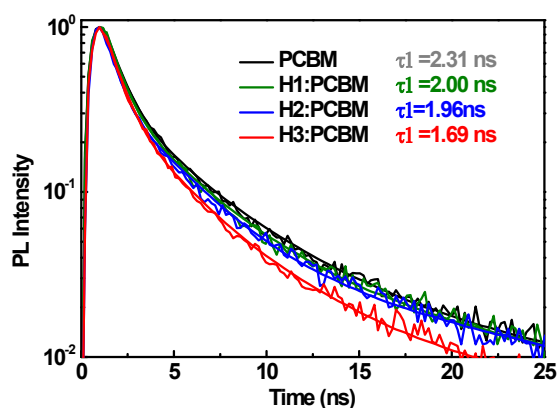


**Figure S8.** Time-resolved PL spectra of the perovskite, perovskite/PCBM, and perovskite/0.05%H3-doped PCBM films.

**Table S2.** Summary of the parameters for the time-resolved PL decay measurements. The fitting process was performed with bi-exponential decay model ( $R(t) = A_1 e^{-t/\tau_1} + A_2 e^{-t/\tau_2}$ ) using the F980 spectrometer operating software.

Meso	A1	$\tau_1$ [ns]	A2	$\tau_2$ [ns]
Perovskite	0.21	1.34±0.08	0.79	33.2±0.1
Perovskite/PCBM	0.86	2.31±0.04	0.14	17.4±0.3
Perovskite/H1:PCBM	0.85	2.00±0.05	0.15	19.2±0.4
Perovskite/H2:PCBM	0.86	1.96±0.05	0.14	21.7±0.5
Perovskite/H3:PCBM	0.85	1.69±0.05	0.15	18.9±0.5

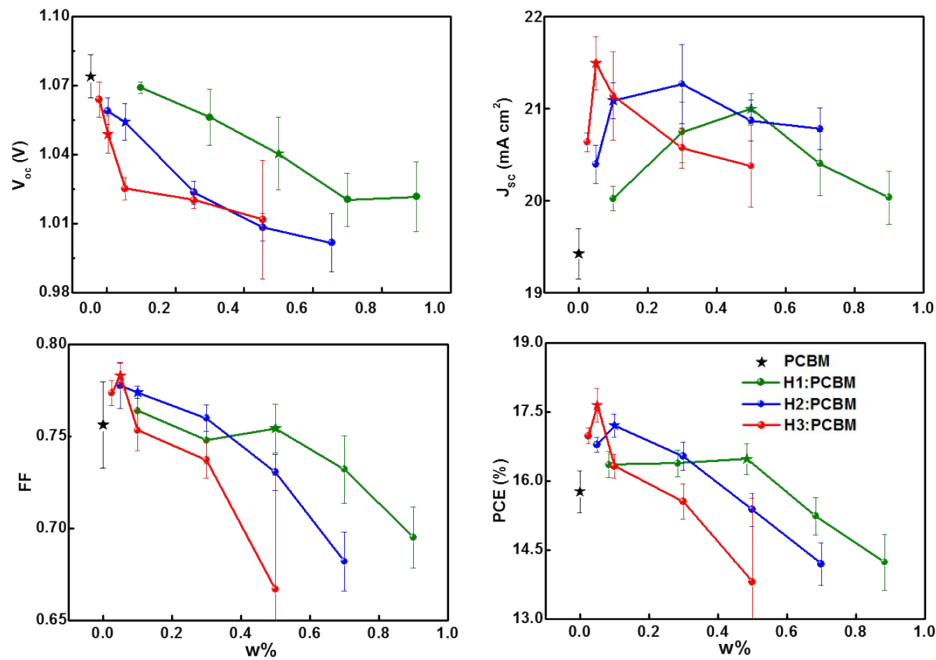


**Figure S9.** Photovoltaic performance of undoped and Hx (H1, H2 and H3) doped devices with different doping ratios.

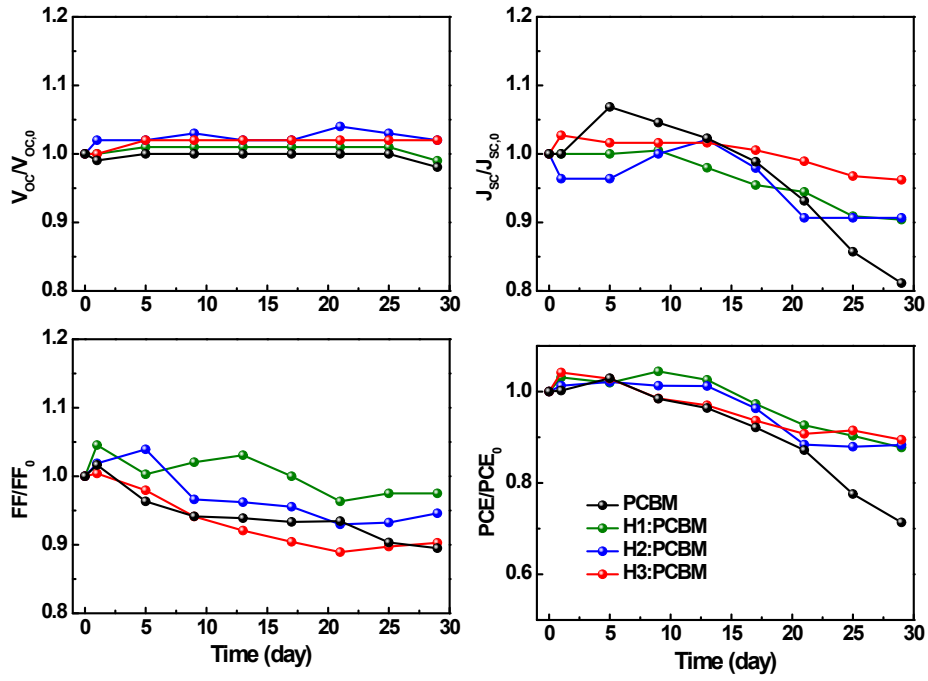
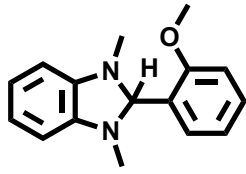
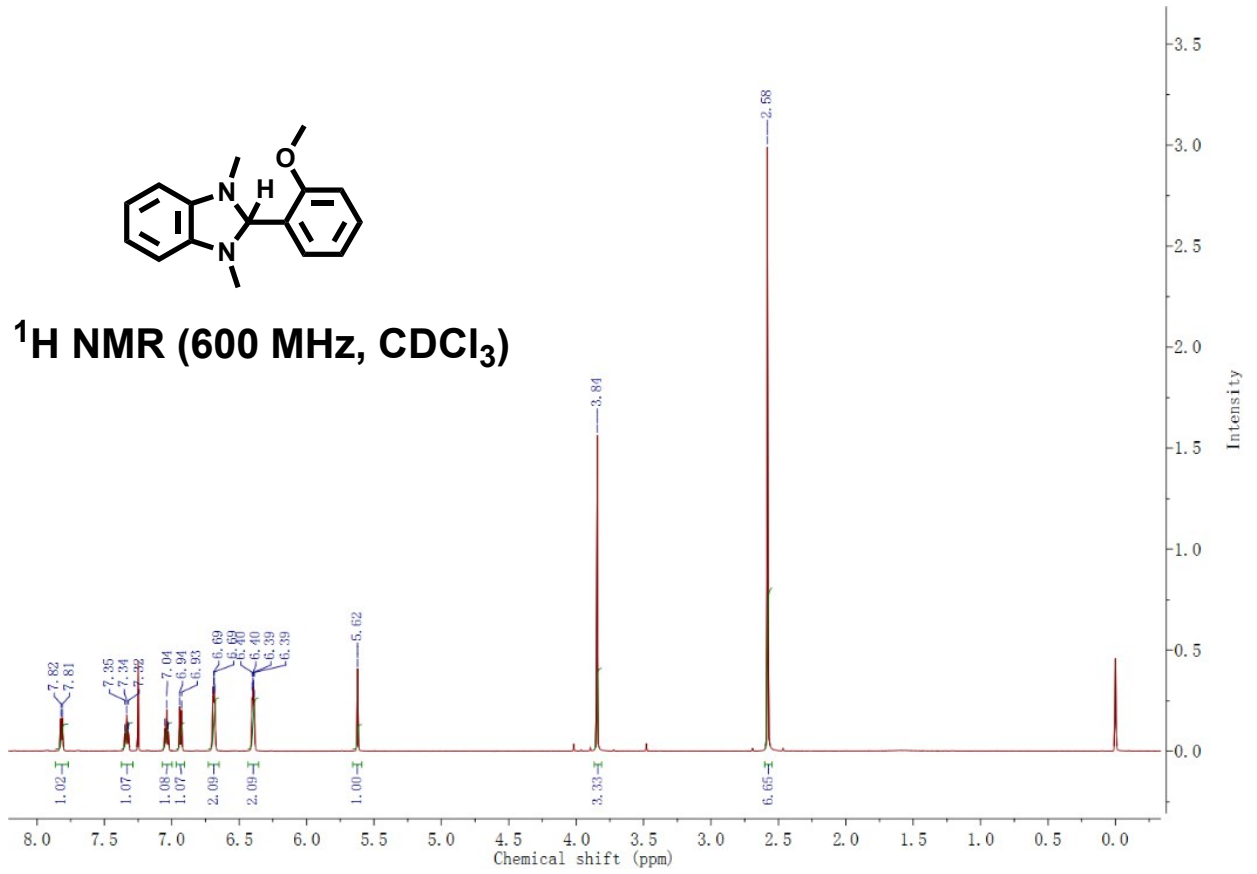


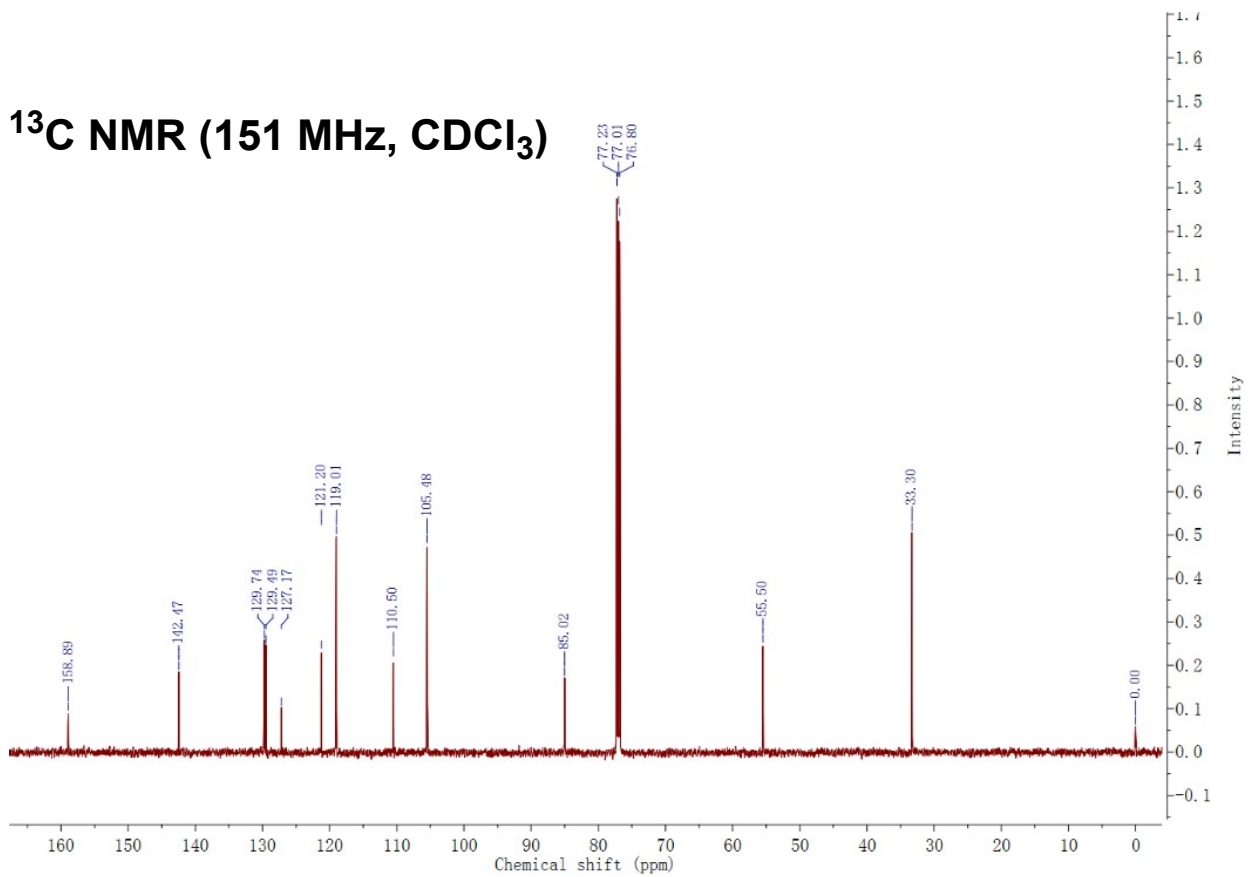
**Figure S10.** Stability of unsealed cells kept in the dark (Temperature= ~25 °C, Relative humidity= ~30%). The content of H1, H2 and H3 are their corresponding optimized doping ratios of 0.5, 0.1, 0.05 w%, respectively.

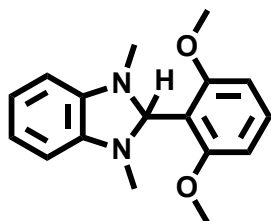


### $^1\text{H}$ NMR (600 MHz, $\text{CDCl}_3$ )

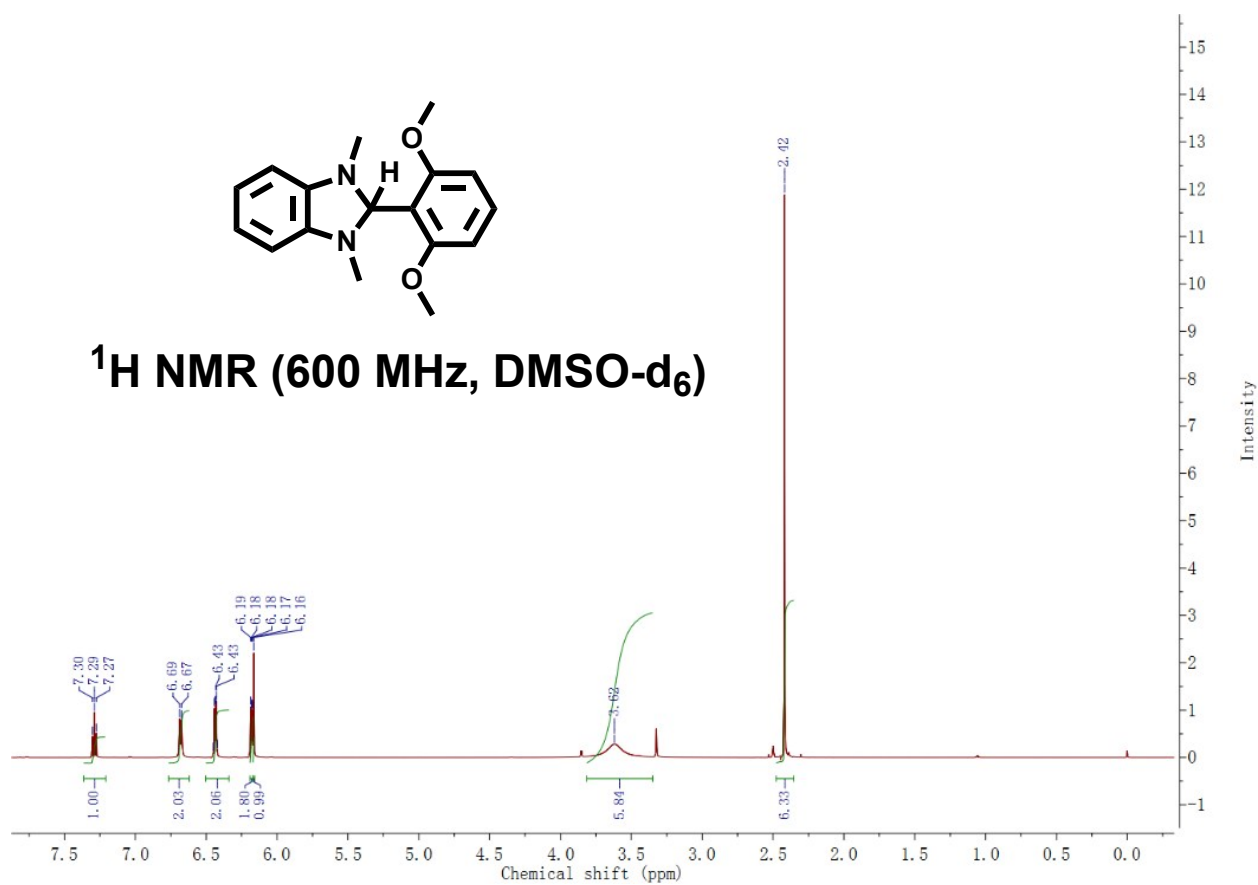


### $^{13}\text{C}$ NMR (151 MHz, $\text{CDCl}_3$ )

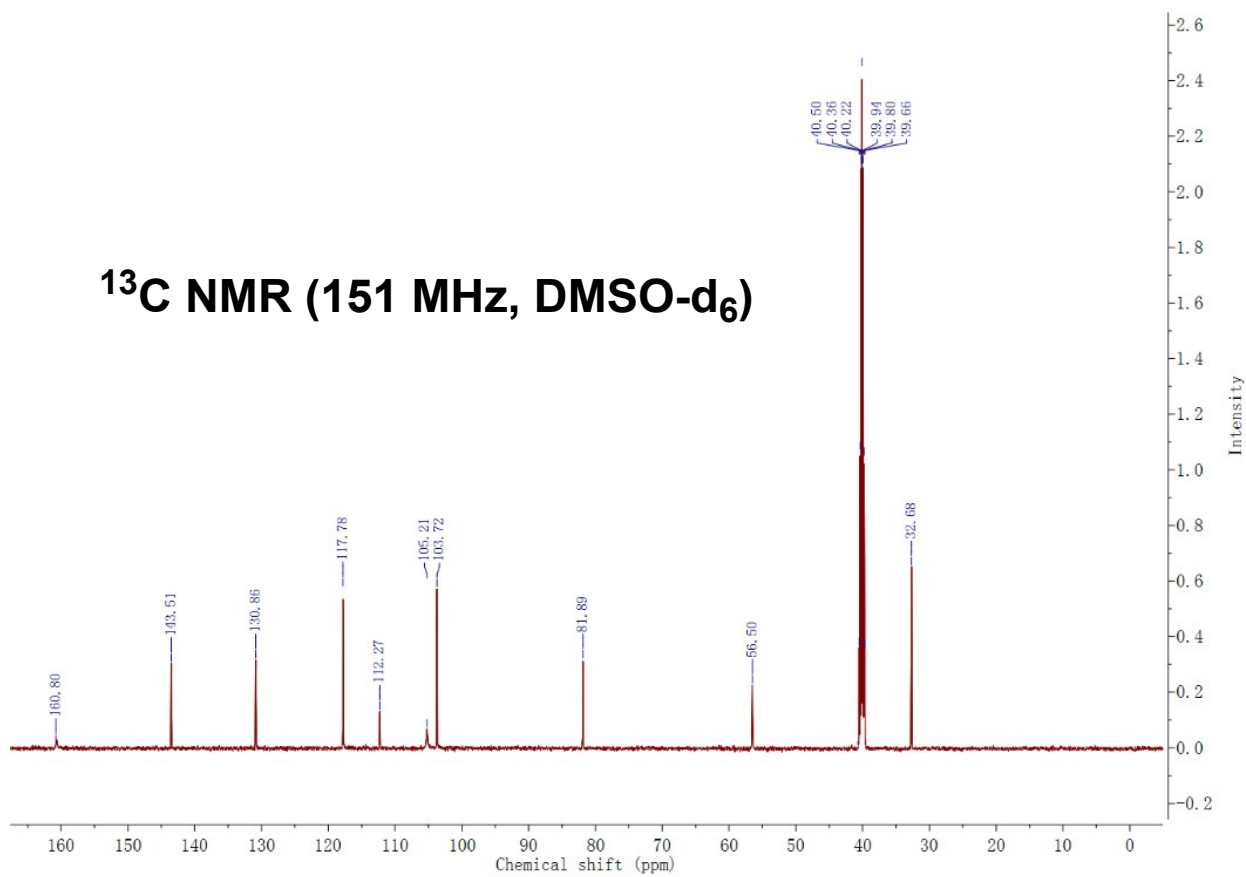


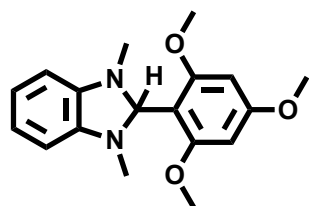


### $^1\text{H}$ NMR (600 MHz, DMSO- $d_6$ )

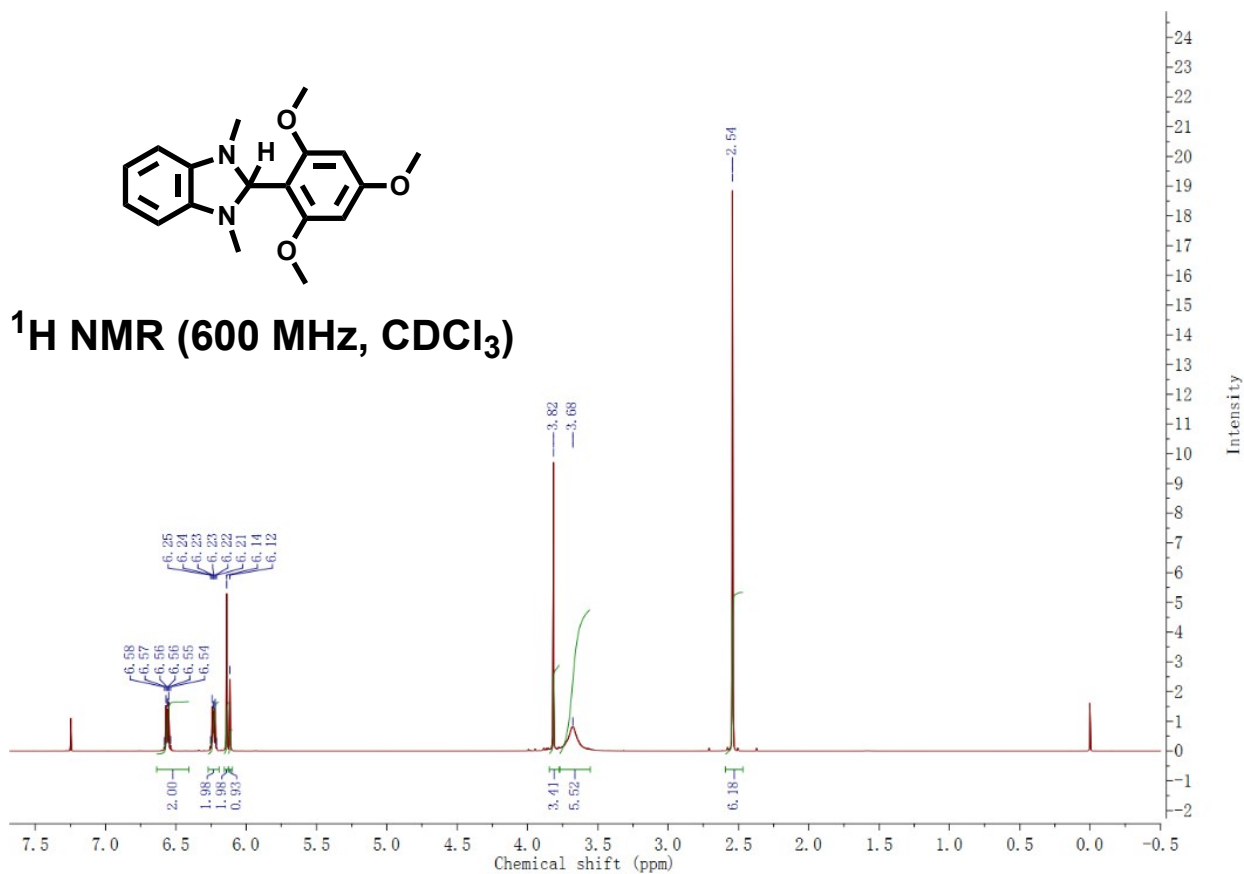


### $^{13}\text{C}$ NMR (151 MHz, DMSO- $d_6$ )





**$^1\text{H}$  NMR (600 MHz,  $\text{CDCl}_3$ )**



**$^{13}\text{C}$  NMR (151 MHz,  $\text{CDCl}_3$ )**

